RESEARCH

Analyzing the topological properties of resting-state brain function network connectivity based on graph theoretical methods in patients with high myopia

Bin Wei[1†] , Xin Huang[2†] , Yu Ji[1] , Wen-Wen Fu[1] , Qi Cheng[1] , Ben-Liang Shu[1] , Qin-Yi Huang[1] , Hua Chai[1] , Lin Zhou[1] , Hao-Yu Yuan[1] and Xiao-rong Wu[1*]

Abstract

Aim Recent imaging studies have found significant abnormalities in the brain's functional or structural connectivity among patients with high myopia (HM), indicating a heightened risk of cognitive impairment and other behavioral changes. However, there is a lack of research on the topological characteristics and connectivity changes of the functional networks in HM patients. In this study, we employed graph theoretical analysis to investigate the topological structure and regional connectivity of the brain function network in HM patients.

Methods We conducted rs-fMRI scans on 82 individuals with HM and 59 healthy controls (HC), ensuring that the two groups were matched for age and education level. Through graph theoretical analysis, we studied the topological structure of whole-brain functional networks among participants, exploring the topological properties and differences between the two groups.

Results In the range of 0.05 to 0.50 of sparsity, both groups demonstrated a small-world architecture of the brain network. Compared to the control group, HM patients showed significantly lower values of normalized clustering coefficient (γ) ($P = 0.0101$) and small-worldness (σ) ($P = 0.0168$). Additionally, the HM group showed lower nodal centrality in the right Amygdala ($P < 0.001$, Bonferroni-corrected). Notably, there is an increase in functional connectivity (FC) between the saliency network (SN) and Sensorimotor Network (SMN) in the HM group, while the strength of FC between the basal ganglia is relatively weaker ($P < 0.01$).

Conclusion HM Patients exhibit reduced small-world characteristics in their brain networks, with significant drops in γ and σ values indicating weakened global interregional information transfer ability. Not only that, the topological properties of the amygdala nodes in HM patients significantly decline, indicating dysfunction within the brain network. In addition, there are abnormalities in the FC between the SN, SMN, and basal ganglia networks in HM

†Bin Wei and Xin Huang contributed equally to this work.

*Correspondence:
Xiao-rong Wu
wxr98021@126.com

Full list of author information is available at the end of the article

patients, which is related to attention regulation, motor impairment, emotions, and cognitive performance. These findings may provide a new mechanism for central pathology in HM patients.

Keywords High myopia, Graph theory, Network-based statistics, Brain function, Topological organization

Introduction

In the past decade or so, due to genetic factors and excessive eye use by adolescents, the myopia rate among teenagers has significantly increased from less than 20% to over 90%. About 20% of people are highly myopic, with a significant surge in myopia incidence [1–6]. High myopia (HM), a visual disorder characterized by a refractive error of over 600 degrees and an elongated eyeball, has become increasingly common in China. Although there are many methods available to correct myopia, pathological myopia caused by HM may lead to serious complications and even blindness, and may also affect brain structure [7, 8]. However, current research has only provided a limited understanding of the topological structure of brain networks in HM patients.

With the development of imaging technology, Functional magnetic resonance imaging (fMRI) has been widely used in research on the brain of various diseases, reflecting mainly the activity of brain regions and the functional connectivity (FC) status between brain regions [9, 10]. Cheng observed a significant reduction in Voxel-Mirrored Homotopic Connectivity (VMHC) values in the fusiform gyrus and putamen of HM patients, indicating that abnormal visual experience may affect their visual recognition function [11]. Wang observed that the DKI-derived Kurtosis parameter in HM patients showed a negative correlation with illness duration, indicating microstructural changes in brain regions related to visual and motor conduction functions [39]. Additionally, Zhai used resting-state FC density (FCD) mapping to find a decrease in FCD in areas such as the inferior temporal gyrus, superior marginal gyrus, and lateral prefrontal cortex in HM patients. These findings help to understand the attention deficit of HM [12]. Previously, we also observed abnormal changes in the FC of the hippocampus in HM patients, which may lead to damage in areas such as emotion, behavior, cognitive memory, and related aspects [13]. The findings above indicate that the alterations in FC in the brain regions of HM patients are not limited to a single brain region, but rather involve related brain regions such as those related to emotions, cognition, and behavior at the whole-brain level. This suggests that further exploration of the central nervous mechanism of HM may require a more comprehensive analysis.

The brain is a complex network that facilitates the separation and integration of information processing [19]. Graph theoretical analysis is used to study and analyze the relationships between nodes and edges in a graph, with the aim of understanding and comprehending the working patterns and information transmission characteristics of the brain through quantitative analysis of network features, such as global and node properties [14, 40]. The global attributes of the network are the description of the connectivity of the whole-brain network, which mainly includes clustering coefficient (Cp) and local efficiency (E_{loc}) to measure the local information transfer efficiency and fault tolerance, shortest path length (Lp) and global efficiency (E_{glob}) to measure the global information transfer efficiency and integration ability, small worldness (σ). Node properties are used to describe the connectivity between brain regions, including node degree, node efficiency, and betweenness centrality. These parameters can be used to identify hub nodes that play a role as bridges in information transmission in the network [41]. The combination of graph theory and MRI technology has been widely used in recent years for analyzing brain networks, and this method has been applied to various diseases [15–17]. Wang discovered that patients with HM have lower values of Eloc and Cp compared to healthy individuals, and there are significant changes in the white matter structural network. The information transmission efficiency in the brain remains relatively unchanged, with the influence of Lp being relatively minor. This suggests that abnormal visual information input may lead to changes in brain structure, resulting in functional reorganization [18]. However, research on HM using fMRI based on graph theoretical analysis techniques is still in its early stages, and it is currently unclear whether HM patients exhibit abnormal node centrality and functional connectivity. Using resting state functional magnetic resonance imaging (rs-fMRI) combined with graph theoretical analysis methods can comprehensively study the changes in the complex networks of HM at the whole-brain level.

The aim of our study is to investigate the topological organization differences in brain functional connectivity among HM patients. We hypothesize that visual impairment, emotional processing, and cognitive dysfunction in HM patients may be related to the disruption of network topology organization.

Materials and methods

Participants

During the period from August to December 2021, the First Affiliated Hospital of Nanchang University recruited a total of 385 participants, of which 254 were excluded. Among the remaining 141 eligible subjects, there were 82 HM patients and 59 healthy controls, who were

Wei *et al. BMC Ophthalmology*   (2024) 24:315

Page 3 of 10

matched according to their gender, age, and educational background.

Subject Requirements: (1) Myopia of both eyes greater than 600 degrees; (2) Corrected visual acuity greater than 1.0 (3) No special findings on ophthalmic examinations such as fundus photography, B-scan ultrasound, optical coherence tomography (4) Ability to tolerate magnetic resonance imaging (MRI) (5) No other special illnesses.

Exclusion criteria: (1) history of significant eye diseases, such as eye trauma, retinal detachment, diabetic retinopathy, glaucoma, etc.; (2) history of previous eye surgery; (3) presence of brain diseases, such as brain hemorrhage.

Inclusion criteria for HCs: (1) visual acuity measured by eye examination greater than 1.0; (2) tolerance to MRI examination (3) absence of any eye or systemic diseases.

MRI acquisition

All participants underwent scanning using the 3-Tesla-Trio MRI scanner system (Trio Tim, Siemens Healthineers, Erlangen, Germany) at the First Affiliated Hospital of Nanchang University in China.T1 weighted imaging scanning parameters: repetition time (TR)=1900 ms, echo time (TE)=2.26 ms, flip angle=12°, number of sagittal slices=176, field of view (FOV)=240×240 mm2, slice thickness=1 mm without gap, acquisition matrix=256×256.

The Turbo spin-echo sequence is used for T2WI scanning, with the following parameters: TR=5100 ms, TE=117 ms, number of axial slices=22, slice thickness=6.5 mm, FOV=240×240 mm^2, matrix=416×416, echo train length=11.

All participants were informed to close their eyes during the MRI scan, wear earplugs, relax their bodies, and not engage in any thoughts.

Data preprocessing

The fMRI data preprocessing was carried out using the Data Processing & Analysis of Brain Imaging toolbox, which is based on SPM8 implemented in MATLAB R2013a. Follow these steps: (1) Convert data from DICOM format to NIFTI format, and remove data from the first 10 time points to avoid the influence of factors such as machine instability during initial startup. (2) The remaining images were time-corrected, volume analysis of function, and head motion correction. Data that have undergone calibration and still have a translation motion of more than 2 mm or rotation motion of more than 2 degrees were removed. (3) Spatial normalization: T1 structural co-registration segmentation and alignment method was used to align the data, and the obtained resting-state data were resampled to a voxel size of 3 mm x 3 mm x 3 mm. (4) Spatial smoothing: spatial smoothing was performed on the standardized imaging data, and

the half-height full-width was set to 6 mm. (5) De-linear drift: The linear regression method is used to remove the linear drift phenomenon caused by thermal noise, such as the heat generated by the MRI scanner. (6) Bandpass filtering (from 0.1 to 0.8 Hz) was used to extract imaging data within this frequency range, thus eliminating the influence of physiological noise.

Network construction

Using the graph theory analysis tool GRETNA(http://www.nitrc.org/projects/gretna/), individual brain regions are usually referred to as nodes, and connections between these regions are referred to as edges. Based on the automatic anatomical labeling (AAL) atlas (Table S1), the brain is symmetrically divided into 90 regions of interest (ROI) [46]. Then, the average time series between all nodes is calculated to define the edges in the network, resulting in a 90×90 correlation matrix. This matrix is converted to a binary matrix, and Fisher's r-to-z transformation is applied to each matrix to improve the data distribution for parametric statistical analysis. The method of selecting based on a sparse degree threshold is used, and the range of sparse degree is set to 0.05~0.50, with a step size of 0.01, to estimate the sparse characteristics of the small world and the number of false edges as little as possible. We calculate the Area Under the Curve (AUC) of network global and node topological attribute indicators within this sparsity range to perform statistical descriptions to reduce the impact of potential biases from any single threshold value.

Network analysis

After constructing the corresponding functional network, the global and node topology attribute metrics are calculated. All metrics concepts are listed in Table 1.

The global network metrics included: (1) clustering coefficient (Cp); (2) characteristic path length (Lp) (3) normalized clustering coefficient (γ) (4) normalized characteristic path length (λ) (5) small-worldness (σ) (6) global efficiency (E_{glob}) (7) local efficiency (E_{loc}).

The nodal network metrics included: (1) Nodal Efficiency (Ne); (2) Degree centrality (Dc) (3) Betweeness centrality (Bc) (4) Nodal Clustering Coefficient (NCp) (5) Nodal Local Efficiency (NLe) (6) Nodal Shortest Path (NLp).

Statistical analysis

Using χ^2 test and independent sample t-test, the demographic and clinical data of two groups of subjects were statistically analyzed with SPSS software version 29.0.

In the range of 0.05–0.50 for sparsity, with a step size of 0.01, we used a two-sample t-test to compare differences between two groups for 7 global network indicators($P<0.05$)and 6 regional node

Wei *et al. BMC Ophthalmology*   (2024) 24:315

Page 4 of 10

Table 1 Descriptions of the network metrics examined in this study

Attribute	Character	Description
Global metrics		
Clustering coefficient	Cp	The extent of local interconnectivity or cliquishness of a network
Characteristic path length	Lp	The extent of overall communication efficiency of a network
Gamma	γ	The deviation of Cp of a network from those of surrogate random networks
Lambda	λ	The deviation of Lp of a network from those of surrogate random networks
Sigma	σ	The small-worldness indicating the extent of a network between randomness and order
Global efficiency	E_{glob}	The ability of a network to transmit information at the local level
Local efficiency	E_{loc}	The ability of a network to transmit information at the global level
Nodal metrics		
NodalEfficiency	Ne	The ability of a node to propagate information with the other nodes in a network
Degree centrality	Dc	The number of edges linked to a node
Betweeness centrality	Bc	The influence that one node has over the flow of information between all other nodes in the network
Nodal Clustering Coefficient	NCp	The ratio of the actual number of edges in the subnetwork to the maximum possible number of edges.
NodalLocalEfficiency	NLe	The efficiency of local information transfer between nodes.
NodalShortestPath	NLp	The shortest connection between two nodes.

Abbreviations: Cp, clustering coefficient; Lp, characteristic path length; γ, normalized clustering coefficient; λ, normalized characteristic path length; σ, scalar smallworldness; E_{glob}, global efficiency; E_{loc}, local efficiency

Table 2 Demographic and clinical characteristics of HM and HC groups

Characteristic	HM	HC
Men/women	37/45	24/35
Age (years)	26.23±5.462	25.78±3.102
ALM (OD)	26.67±0.874	23.90±0.971
ALM (OS)	26.58±0.985	23.74±0.693
Population of interest	276	109
Meet the exclusion criteria	194	60
Eligible for inclusion criteria	82	59

Abbreviations: HM, high myopia; HC, healthy control; ALM, axial length; OD, oculus dexter; OS, oculus sinister

Table 3 Significant differences in integrated global network parameters between two groups

Network parameters	HM (mean)	HC (mean)	t-Values	*p*-Values
Cp	0.251	0.254	-1.317	0.1897
Lp	0.836	0.835	1.908	0.8489
γ	1.065	1.096	**-2.608**	**0.0101***
λ	0.490	0.490	-2.455	0.8063
σ	0.944	0.968	**-2.419**	**0.0168***
E_{glob}	0.263	0.262	5.463	0.5856
E_{loc}	0.337	0.340	-1.754	0.0814

Notes The small-world parameters and network efficiency parameters comparisons in patients with HM and HCs. Both the HM and HCs exhibited small-world attribute. The HM group showed decreased exhibited increased Lp, E_{glob}, and decreasedCp, E_{loc} γ, and λ. The symbol "*" denotes *p* < 0.05. (two sample t-tests, *p* < 0.05). The significance of bold values indicate the *p* < 0.05 and the corresponding t-values

Abbreviations Cp, clustering coefficient; Lp, characteristic path length; γ, normalized clustering coefficient; λ, normalized characteristic path length; σ, scalar smallworldness; E_{glob}, global efficiency; E_{loc}, local efficiency; HM, high myopia; HC, health control

parameters(*P* < 0.05, Bonferroni-corrected), and calculate the AUC for each indicator for statistical analysis.

Using a network-based statistics (NBS) method(http://www.nitrc.org/projects/nbs/) to analyze the brain functional connectivity regions that display nodal characteristics differences between groups, and calculated the significance of each region using independent two-sample t-tests and nonparametric permutation methods with 10,000 permutations.

Results

Basic information

This study included a total of 82 HM patients (37 males, 45 females, with a mean age of 26.23±5.462 years) and 59 HCs (24 males, 35 females, with a mean age of 25.78±3.102 years). Demographic and clinical characteristics are shown in Table 2.

Small-world changes in brain functional networks.

The thresholds between defined as 0.05 and 0.50 were used, with a step size of 0.01, and both the HM group and HC group demonstrated small-world network properties (γ > 1, λ ≈ 1, σ > 1). There were significant reductions in the γ(*P*=0.0101) and σ(*P*=0.0168) in HM patients compared to the HC group, with no significant differences observed between the two groups for the remaining topological small-world parameters. (Table 3; Fig. 1).

Nodal changes in brain functional networks.

Comparison between two groups on five nodal metrics showed no statistically significant difference except for Nodal Local Efficiency. HM patients showed significantly lower nodal centralities in the right Amygdala compared to HC (*P* < 0.001, Bonferroni-corrected). (Table 4; Fig. 2).

Graph theory analysis of HM related functional connection alterations.

Based on the NBS research method, it was found that there were significant changes in 16 nodes and 19 functional connections in the HM group compared to the HC group (*P* < 0.01).HM patients displayed significantly
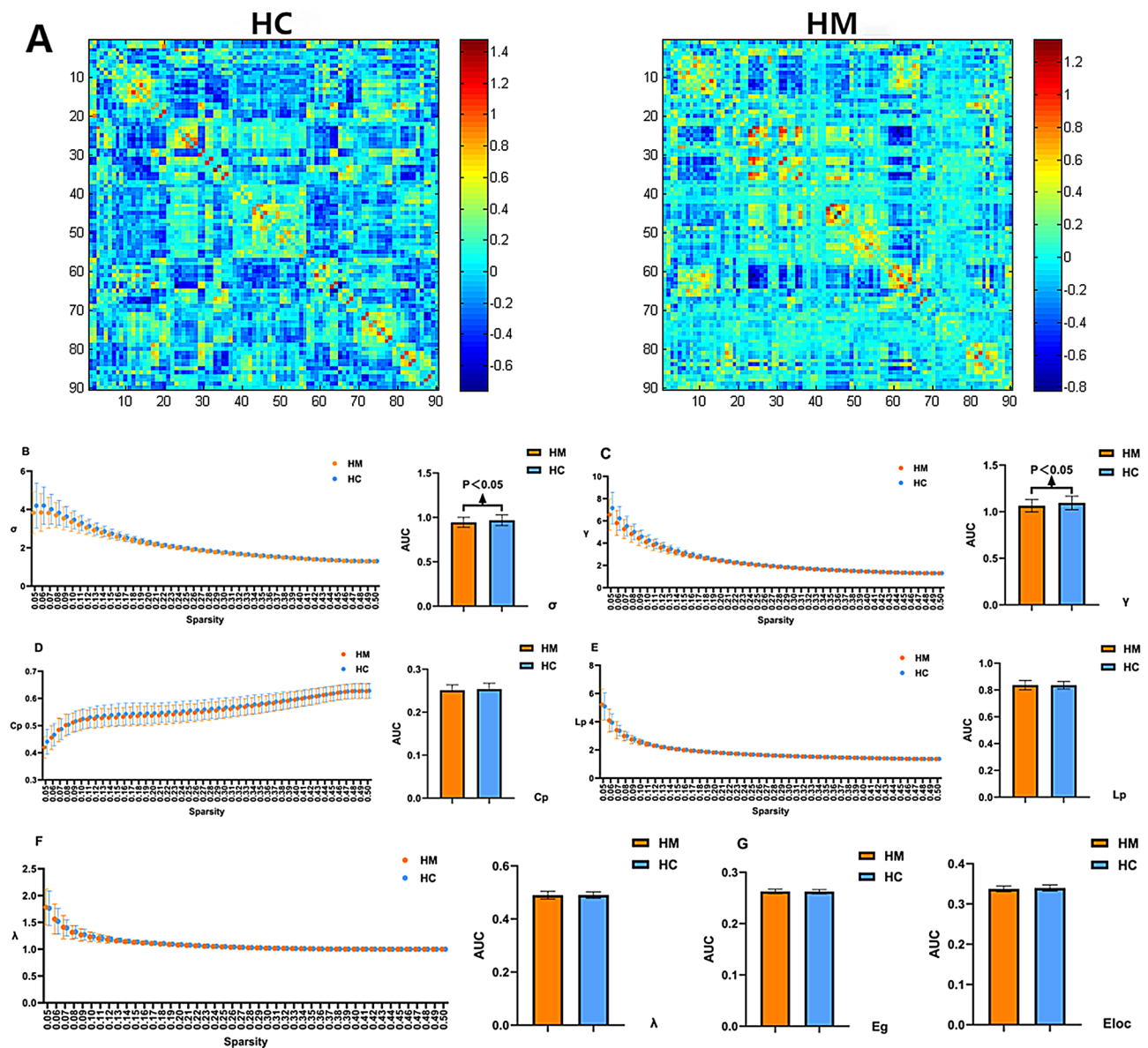
Fig. 1 Mean functional connectivity strengths and global network properties between the HM and HC groups. The figure shows that within the defined sparsity range (0.05 < S < 0.50), both the HM and HC groups exhibit typical small-world properties ($\gamma = Cp_{real}/Cp_{rand} > 1, \lambda = Lp_{real}/Lp_{rand} \approx 1$). The circles represent the average values of HM and HC, and the error bars represent the standard error of each group's states.(**A**) The mean Pearson correlation matrices of the HC and HM group.(**B-F**) Small-world network architecture and AUC value.(**G**)AUC value of network efficiency . Abbreviations: Cp= clustering coefficient; Lp= characteristic path length; λ= normalized shortest path length;γ= normalized clustering coefficient;σ=small-worldness; E_{glob} = global efficiency; E_{loc} = local efficiency AUC, area under curve; HM, High myopia; HC, health control

Table 4 Between-group differences in nodal characteristics in patients with HM and HC

	Brain regions	Nodal Local Efficiency	
		t-Values	*p*-Values
HM < HC	Right Amygdala	-3.886	0.0001

Note: Bonferroni correction was applied to each nodal characteristic, the p-value thresholds for nodal characteristics were 0.01.The significance of bold values indicate the *p* < 0.001

Abbreviations: HM, high myopia; HC, health control

higher FC values in the regions of Lenticular nucleus-putamen(PUT), Parahippocampal gyrus(PHG), Median cingulate and paracingulate gyri(DCG), Superior temporal gyrus(STG), Heschl gyrus(HES), Postcentral gyrus(PoCG)and Precental gyrus(PreCG) compared to HC, while there were significant reductions in FC values in the regions of Lenticular nucleus-putamen(PUT), Inferior frontal gyrus- opercular part(IFGoperc), Caudate nucleus(CAU)and Lenticular nucleus-pallidum(PAL). (Table 5; Fig. 3).
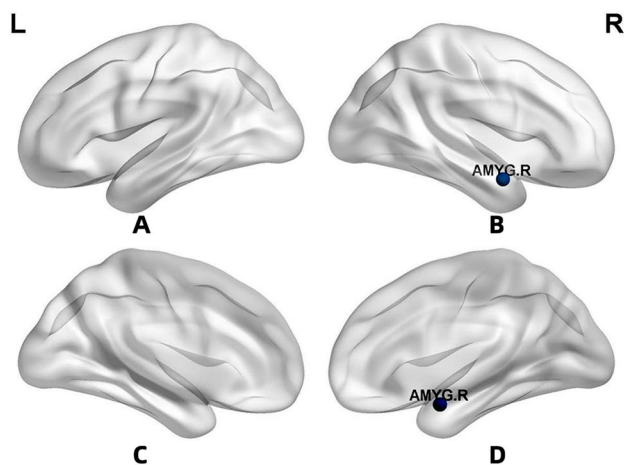
Wei *et al. BMC Ophthalmology*   (2024) 24:315

Page 6 of 10

Fig. 2 Significant nodal characteristics map the differences between two groups Notes:**A** (Left Sagittal View from Midline): The brain's left hemisphere viewed from the midline, split along the sagittal plane, looking outward. **B** (Right Sagittal View from Midline): The brain's right hemisphere viewed from the midline, split along the sagittal plane, looking outward. **C** (Left Lateral Sagittal View): The brain's left hemisphere viewed from the outside, split along the sagittal plane, looking inward. **D** (Right Lateral Sagittal View): The brain's right hemisphere viewed from the outside, split along the sagittal plane, looking inward Blued color indicates decreased nodal characteristics (HM < HC) (*P* < 0.001, Bonferroni-corrected). The HM group had a significant decreased nodal centralities in the AMYG.R

Table 5 Significantly altered functional connectivities in HM patients compared with HCs

Region 1	Category	Region 2	Category	t-Values	*p*-Values
PHG.R	Temporal	PoCG.L	Parietal	3.407	0.0009
DCG.L	Frontal	PUT.L	Subcortical	3.442	0.0008
PreCG.R	Frontal	HES.R	Temporal	3.615	0.0004
DCG.L	Frontal	HES.R	Temporal	3.639	0.0004
DCG.R	Frontal	HES.R	Temporal	4.389	<0.0001
PoCG.L	Parietal	HES.R	Temporal	3.473	0.0007
DCG.L	Frontal	STG.L	Temporal	3.819	0.0002
DCG.R	Frontal	STG.L	Temporal	3.774	0.0002
DCG.L	Frontal	STG.R	Temporal	4.772	<0.0001
DCG.R	Frontal	STG.R	Temporal	4.102	0.0001
IFGoperc.L	Prefontal	CAU.L	Subcortical	-3.522	0.0006
IFGoperc.R	Prefontal	CAU.L	Subcortical	-3.426	0.0008
CAU.R	Subcortical	PUT.L	Subcortical	-3.829	0.0002
CAU.R	Subcortical	PUT.R	Subcortical	-3.940	0.0001
PUT.L	Subcortical	PUT.R	Subcortical	-5.570	<0.0001
CAU.L	Subcortical	PAL.L	Subcortical	-3.572	0.0005
CAU.R	Subcortical	PAL.L	Subcortical	-3.929	0.0001
CAU.L	Subcortical	PAL.R	Subcortical	-3.812	0.0002
CAU.R	Subcortical	PAL.R	Subcortical	-4.176	0.0001

Note NBS method identified a significantly altered network (16 nodes and 19 connections) in HM group relative to HCs. (*P* < 0.01)

Abbreviations PHG, Parahippocampal gyrus; DCG, Median cingulate and paracingulate gyri; PreCG, Precental gyrus; PoCG, Postcentral gyrus; IFGoperc, Inferior frontal gyrus, opercular part; CAU, Caudate nucleus; PUT, Lenticular nucleus, putamen; HES, Heschl gyrus; STG, Superior temporal gyrus; PAL, Lenticular nucleus, pallidum; NBS, network-based statistics; HM, high myopia; HC, health control

Discussion

We constructed a network matrix and used graph theory analysis to explore the topological attributes of abnormal resting-state brain functional networks in HM patients. The research results showed that compared with healthy controls: (1) γ and σ decreased in HM patients; (2) the nodal centralities of the right amygdala decreased; and (3) there was an increase in FC between SN and SMN and an decrease in functional connectivity between regions of the basal ganglia network.

Alterations in global network topology attributes

The working principle of the brain is to quickly understand and process information through the integration and separation of functions [19]. Shu has suggested that small-world properties can achieve the optimal balance between the whole and the local in the brain network, providing a basis for efficient information communication [20]. Cao believes that small-world properties can change accordingly with the occurrence of diseases [21]. Our findings coincide with this notion. In this study, we found that both HM patients and healthy controls exhibit small-world properties within the range of sparsity from 0.05 to 0.50. However, the between-group comparison of global topological indicators, measured by the AUC value, showed that HM patients had significantly decreased σ and γ values. γ is related to the brain network's ability to separate functions [22, 23]. Therefore, lower γ and σ values may indicate impaired small-world properties of the brain network, disrupted functional segregation, and compromised dynamic balance of the brain network.

Alterations in network node topology attributes

In addition to global topological indicators, certain nodes within the brain network have shown changes, indicating abnormalities in the transmission and integration functions of these nodes. These alterations may result in changes to the associated functional networks [27]. By comparing the AUC values of node indicators Ne, NLe, NCp, NLp, Bc, and Dc in two groups of subjects, this study discovered a significant reduction in NLe values specifically within the right amygdala of patients with HM. The amygdala, located in the posterior and medial temporal lobe, is an important component of the SN, a region responsible for generating and processing emotions. It is involved in bottom-up attention towards emotional stimuli and plays a crucial role in cognitive, memory, learning, and decision-making processes [24–26]. Numerous studies consistently demonstrate the strong association between the amygdala and the hippocampus [28]. Additionally, our previous research has also identified functional connectivity abnormalities in the hippocampus [13]. Hence, it is hypothesized that high
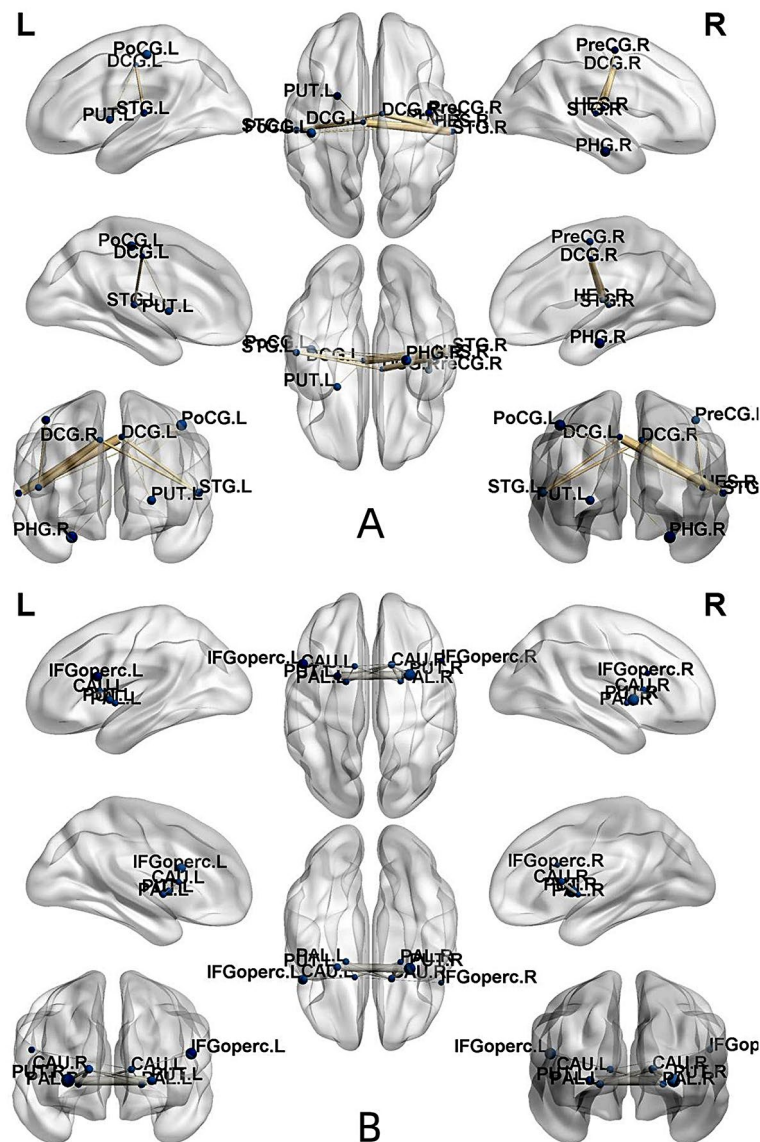
Wei *et al. BMC Ophthalmology*   (2024) 24:315

Page 7 of 10

Fig. 3 Graph theory analysis of alterations in brain functional connectivity. (**A**)Compared to the HC group, the increased brain functional connectivity in patients with HM. (**B**)Compared to HC group, patients with HM have reduced brain functional connectivity. Notes NBS method identified a significantly altered network (16 nodes and 19 connections) in HM group relative to HCs. ($P < 0.01$). The thickness of the line represents the strength of the functional connection. Abbreviations: PHG, Parahippocampal gyrus; DCG, Median cingulate and paracingulate gyri; PreCG, Precental gyrus; PoCG, Postcentral gyrus; IFGoperc, Inferior frontal gyrus, opercular part; CAU, Caudate nucleus; PUT, Lenticular nucleus, putamen; HES, Heschl gyrus; STG, Superior temporal gyrus; PAL, Lenticular nucleus, pallidum ; R, right; L, left

myopia patients may exhibit impairments in cognitive function, emotion regulation, and memory, attributable to the reduced connectivity within the SN.

Functional connectivity

HM patients exhibited varying degrees of functional connectivity changes in 16 nodes and 19 connections. We observed a significant decrease in connectivity within the prefrontal lobe (IFGoperc) and subcortical regions (CAU, PUT, and PAL). The IFG belongs to the DMN and is closely related to the detection, regulation, and cognitive control of emotions. The changes in its activity are

related to the abnormal visual regulation mechanism of HM patients [29–31]. The tail nucleus, shell nucleus, and putamen belong to the basal ganglia network, which plays a crucial role in visually guided decision-making and eye movement control. The damage to the basal ganglia network is also the basis for various movement disorders [32, 33, 41]. A study has found a significant relationship between DMN connectivity and regions within the basal ganglia, indicating that these systems jointly engage in associative learning and memory based on rewards, and may represent crucial connections necessary for adaptive cognition [42]. Shu found changes in the caudate

Wei *et al. BMC Ophthalmology*   (2024) 24:315

Page 8 of 10

nucleus and putamen in blind patients, emphasizing the importance of vision loss in motor control [20]. Similarly, Zikou discovered a decrease in fractional anisotropy (FA) in the caudate nucleus and putamen of glaucoma patients [34]. Currently, there is no research confirming structural changes in the striatum of HM patients. However, we speculate that HM patients may experience cognitive decision-making difficulties and weakness in eye movements.

In addition, there was an increase in FC between the PUT, PHG, DCG, STG, HES, PoCG, and PreCG groups in the HM group, mainly concentrated in the SN and SMN. The SMN primarily synchronizes the processing of sensory input to form a shared sensory experience, whereas the SN plays an indispensable role in the processing of sensorimotor information, overall cognition, and coordination between emotions, pain, and bodily actions [43, 44]. A study found that the density of FC in the SN of individuals with schizophrenia has decreased, while the dynamic increase in connectivity within the SN indicates that Sn dysfunction may be due to a reduction in the stability of internal connections within the network [45]. PHG, STG, and HES are part of the temporal lobe, which is primarily responsible for language function and auditory perception, as well as being involved in long-term memory and emotions [35, 36]. Wu found a reduction in cortical surface thickness in the right STG of HM patients, indicating a possible association with vision [37]. Huang discovered that HM patients had significantly increased GMV in the right parahippocampal gyrus, which could contribute to memory impairments in HM patients [38]. DCG and PreCG are part of the frontal lobe. Wang observed significant changes in BC in the dorsal DCG of HM patients, suggesting alterations in processing functions related to memory, vision, and attention [18]. Our research found that there are widespread connectivity changes in the SMN and SN of the HM group, which may lead to further motor dysfunction and cognitive-emotional deficits.

Limitations

In fact, our study does have some limitations. Firstly, various factors that participants encountered during MRI-related examinations may have influenced the results. Secondly, due to the limited number of participants ultimately included, we did not analyze the correlation between the clinical manifestations of HM and the topological brain tissue characteristics. Additionally, we acknowledge that the impact of the duration of high myopia on brain function changes, which we failed to delve deeply into, may differ from our current findings. When we included demographic variables, we did not include many important variables due to missing data, such as blood pressure, height and BMI, which are all

important factors that may affect our results. Therefore, in future studies, we will try to minimize these problems.

Conclusion

Research has shown that, compared to the HC group, patients with HM experience abnormal changes in the topological organization of their brain's functional connectivity. This mainly manifests in the patients with HM exhibiting reduced levels of γ and σ, a significant decrease in the centrality of the right amygdala node, and abnormal functional connectivity between SN, SMN, and basal ganglia networks. This also relates to a decline in vision and changes in emotional cognition in HM patients. These findings may also provide new perspectives for studying the pathological and physiological mechanisms of HM.

Author contributions

Author contributions included conception and study design (B.W, X.W and X.H), data collection or acquisition (Y.J, W.F and Q.C), statistical analysis (B.W, X.H, B.S and Q.H), interpretation of results (L.Z, H.Y, H.C and X.W), drafting the manuscript work or revising it critically for important intellectual content (B.W, X.H, Y.J, Q.C and X.W) and approval of final version to be published and agreement to be accountable for the integrity and accuracy of all aspects of the work (All authors).

Data availability

The original contributions presented in the study are included in the article, further inquiries can be directed to the corresponding author.

Declarations

Ethical approval

All procedures performed in studies involving human participants were in accordance with the ethical standards of the institutional and/or national research committee and with the 1964 Helsinki declaration and its later amendments or comparable ethical standards. The study protocol was approved by the Medical Research Ethics Committee of The First Affliated Hospital of Nanchang University. All data generated or analyzed during this study from patients are included in this published article. All Patients and guardians were provided consent to publish these pictures.

Consent for publication

Not Applicable.

Author details
[1]Department of Ophthalmology, Jiangxi Medical College, Nanchang University, The 1st Affiliated Hospital, Nanchang, Jiangxi, People's Republic of China
[2]Department of Ophthalmology, Jiangxi Provincial People's Hospital, The First Affiliated Hospital of Nanchang Medical College, Nanchang, Jiangxi, China

References

1. Pan CW, Ramamurthy D, Saw SM. Worldwide prevalence and risk factors for myopia. Ophthalmic Physiol Opt. 2012;32(1):3–16. https://doi.org/10.1111/j.1475-1313.2011.00884.x. PMID: 22150586.
2. Morgan IG, Ohno-Matsui K, Saw SM, Myopia. Lancet. 2012;379(9827):1739-48. https://doi.org/10.1016/S0140-6736(12)60272-4. PMID: 22559900.
3. Zhuang M, Xie H, Zhang Y, Li S, Xiao P, Jiang Y, Zhou H, Chu Z, Zhao J. Prevalence and influence factors for myopia and high myopia in schoolchildren in Shandong, China. Cent Eur J Public Health. 2022;30(3):190–195. https://doi.org/10.21101/cejph.a7158. PMID: 36239368.
4. Jonas JB, Panda-Jonas S. Epidemiologie und Anatomie der Myopie [Epidemiology and anatomy of myopia]. Ophthalmologe. 2019;116(6):499–508. German. https://doi.org/10.1007/s00347-019-0858-6. PMID: 30796602.
5. Dolgin E. The myopia boom. Nature. 2015;519(7543):276-8. https://doi.org/10.1038/519276a. PMID: 25788077.
6. Holden BA, Fricke TR, Wilson DA, Jong M, Naidoo KS, Sankaridurg P, Wong TY, Naduvilath TJ, Resnikoff S. Global Prevalence of Myopia and High Myopia and Temporal Trends from 2000 through 2050. Ophthalmology. 2016;123(5):1036-42. https://doi.org/10.1016/j.ophtha.2016.01.006. Epub 2016 Feb 11. PMID: 26875007.
7. Vongphanit J, Mitchell P, Wang JJ. Prevalence and progression of myopic retinopathy in an older population. Ophthalmology. 2002;109(4):704 – 11. https://doi.org/10.1016/s0161-6420(01)01024-7. PMID: 11927427.
8. Wong TY, Ferreira A, Hughes R, Carter G, Mitchell P. Epidemiology and disease burden of pathologic myopia and myopic choroidal neovascularization: an evidence-based systematic review. Am J Ophthalmol. 2014;157(1):9–25.e12. doi: 10.1016/j.ajo.2013.08.010. Epub 2013 Oct 5. PMID: 24099276.
9. Rubinov M, Sporns O. Complex network measures of brain connectivity: uses and interpretations. NeuroImage. 2010;52(3):1059–69. https://doi.org/10.1016/j.neuroimage.2009.10.003. Epub 2009 Oct 9. PMID: 19819337.
10. Sporns O. Structure and function of complex brain networks. Dialogues Clin Neurosci. 2013;15(3):247–62. https://doi.org/10.31887/DCNS.2013.15.3/osporns. PMID: 24174898; PMCID: PMC3811098.
11. Cheng Y, Chen XL, Shi L, Li SY, Huang H, Zhong PP, Wu XR. Abnormal functional connectivity between cerebral hemispheres in patients with high myopia: a resting FMRI study based on Voxel-Mirrored Homotopic Connectivity. Front Hum Neurosci. 2022;16:910846. https://doi.org/10.3389/fnhum.2022.910846. PMID: 35814958; PMCID: PMC9259881.
12. Zhai L, Li Q, Wang T, Dong H, Peng Y, Guo M, Qin W, Yu C. Altered functional connectivity density in high myopia. Behav Brain Res. 2016;303:85–92. https://doi.org/10.1016/j.bbr.2016.01.046. Epub 2016 Jan 22. PMID: 26808608.
13. Wei B, Fu WW, Ji Y, Cheng Q, Shu BL, Huang QY, Wu XR. Exploration of hippocampal functional connectivity alterations in patients with high myopia via seed-based functional connectivity analysis. Clin Ophthalmol. 2023;17:3443–51. PMID: 38026590; PMCID: PMC10656840.
14. Zhao L, Guan M, Zhu X, Karama S, Khundrakpam B, Wang M, Dong M, Qin W, Tian J, Evans AC, Shi D. Aberrant topological patterns of structural cortical networks in Psychogenic Erectile Dysfunction. Front Hum Neurosci. 2015;9:675. PMID: 26733849; PMCID: PMC4683194.
15. Yun JY, Kim YK. Graph theory approach for the structural-functional brain connectome of depression. Prog Neuropsychopharmacol Biol Psychiatry. 2021;111:110401. https://doi.org/10.1016/j.pnpbp.2021.110401. Epub 2021 Jul 12. PMID: 34265367.
16. Khazaee A, Ebrahimzadeh A, Babajani-Feremi A. Identifying patients with Alzheimer's disease using resting-state fMRI and graph theory. Clin Neurophysiol. 2015;126(11):2132–41. https://doi.org/10.1016/j.clinph.2015.02.060. Epub 2015 Apr 1. PMID: 25907414.
17. Farahani FV, Karwowski W, D'Esposito M, Betzel RF, Douglas PK, Sobczak AM, Bohaterewicz B, Marek T, Fafrowicz M. Diurnal variations of resting-state fMRI data: a graph-based analysis. NeuroImage. 2022;256:119246. https://doi.org/10.1016/j.neuroimage.2022.119246. Epub 2022 Apr 25. PMID: 35477020; PMCID: PMC9799965.
18. Wang H, Wen H, Li J, Chen Q, Li S, Wang Z. Disrupted topological organization of white matter structural networks in high myopia patients revealed by diffusion kurtosis imaging and tractography. Front Neurosci. 2023;17:1158928. https://doi.org/10.3389/fnins.2023.1158928. PMID: 37425009; PMCID: PMC10324656.
19. Tononi G, Edelman GM, Sporns O. Complexity and coherency: integrating information in the brain. Trends Cogn Sci. 1998;2(12):474 – 84. https://doi.org/10.1016/s1364-6613(98)01259-5. PMID: 21227298.
20. Shu N, Liu Y, Li J, Li Y, Yu C, Jiang T. Altered anatomical network in early blindness revealed by diffusion tensor tractography. PLoS ONE. 2009;4(9):e7228. https://doi.org/10.1371/journal.pone.0007228. PMID: 19784379; PMCID: PMC2747271.
21. Cao Q, Shu N, An L, Wang P, Sun L, Xia MR, Wang JH, Gong GL, Zang YF, Wang YF, He Y. Probabilistic diffusion tractography and graph theory analysis reveal abnormal white matter structural connectivity networks in drug-naive boys with attention deficit/hyperactivity disorder. J Neurosci. 2013;33(26):10676-87. https://doi.org/10.1523/JNEUROSCI.4793-12.2013. PMID: 23804091; PMCID: PMC6618487.
22. Sporns O, Tononi G, Kötter R. The human connectome: a structural description of the human brain. PLoS Comput Biol. 2005;1(4):e42. https://doi.org/10.1371/journal.pcbi.0010042. PMID: 16201007; PMCID: PMC1239902.
23. Liao X, Vasilakos AV, He Y. Small-world human brain networks: Perspectives and challenges. Neurosci Biobehav Rev. 2017;77:286–300. https://doi.org/10.1016/j.neubiorev.2017.03.018. Epub 2017 Apr 5. PMID: 28389343.
24. Prather MD, Lavenex P, Mauldin-Jourdain ML, Mason WA, Capitanio JP, Mendoza SP, Amaral DG. Increased social fear and decreased fear of objects in monkeys with neonatal amygdala lesions. Neuroscience. 2001;106(4):653-8. https://doi.org/10.1016/s0306-4522(01)00445-6. PMID: 11682152.
25. Gangopadhyay P, Chawla M, Dal Monte O, Chang SWC. Prefrontal-amygdala circuits in social decision-making. Nat Neurosci. 2021;24(1):5–18. https://doi.org/10.1038/s41593-020-00738-9. Epub 2020 Nov 9. PMID: 33169032; PMCID: PMC7899743.
26. Ortiz S, Latsko MS, Fouty JL, Dutta S, Adkins JM, Jasnow AM. Anterior Cingulate Cortex and ventral hippocampal inputs to the Basolateral Amygdala selectively Control Generalized Fear. J Neurosci. 2019;39(33):6526–39. https://doi.org/10.1523/JNEUROSCI.0810-19.2019. Epub 2019 Jun 17. PMID: 31209172; PMCID: PMC6697404.
27. Boccaletti S, Latora V, Moreno Y, et al. Complex networks: structure and dynamics. Phys Rep. 2006;424(4/5):175–308.
28. Pang R, Zhan Y, Zhang Y, Guo R, Wang J, Guo X, Liu Y, Wang Z, Li K. Aberrant functional Connectivity Architecture in participants with chronic insomnia disorder accompanying cognitive dysfunction: a Whole-Brain, Data-Driven Analysis. Front Neurosci. 2017;11:259. https://doi.org/10.3389/fnins.2017.00259. PMID: 28553199; PMCID: PMC5425485.
29. Urgesi C, Mattiassi AD, Buiatti T, Marini A. Tell it to a child! A brain stimulation study of the role of left inferior frontal gyrus in emotion regulation during storytelling. NeuroImage. 2016;136:26–36. https://doi.org/10.1016/j.neuroimage.2016.05.039. Epub 2016 May 14. PMID: 27188219.
30. Jastorff J, De Winter FL, Van den Stock J, Vandenberghe R, Giese MA, Vandenbulcke M. Functional dissociation between anterior temporal lobe and inferior frontal gyrus in the processing of dynamic body expressions: insights from behavioral variant frontotemporal dementia. Hum Brain Mapp. 2016;37(12):4472–86. Epub 2016 Aug 11. PMID: 27510944; PMCID: PMC6867423.
31. Zhang X, Liu L, Yang F, Liu Z, Jin X, Han S, Zhang Y, Cheng J, Wen B. Neurovascular coupling dysfunction in high myopia patients: Evidence from a multi-modal magnetic resonance imaging analysis. J Neuroradiol. 2023 Sep 29:S0150-9861(23)00242-0. doi: 10.1016/j.neurad.2023.09.005. Epub ahead of print. PMID: 37777086.
32. Yin X, Chen L, Ma M, Zhang H, Gao M, Wu X, Li Y. Altered brain structure and spontaneous functional activity in children with concomitant Strabismus. Front Hum Neurosci. 2021;15:777762. https://doi.org/10.3389/fnhum.2021.777762. PMID: 34867247; PMCID: PMC8634149.

33. Moss MM, Zatka-Haas P, Harris KD, Carandini M, Lak A. Dopamine axons in dorsal striatum Encode Contralateral Visual Stimuli and choices. J Neurosci. 2021;41(34):7197–205. https://doi.org/10.1523/JNEUROSCI.0490-21.2021. Epub 2021 Jul 12. PMID: 34253628; PMCID: PMC8387116.

34. Zikou AK, Kitsos G, Tzarouchi LC, Astrakas L, Alexiou GA, Argyropoulou MI. Voxel-based morphometry and diffusion tensor imaging of the optic pathway in primary open-angle glaucoma: a preliminary study. AJNR Am J Neuroradiol. 2012;33(1):128–34. https://doi.org/10.3174/ajnr.A2714. Epub 2011 Nov 24. PMID: 22116110; PMCID: PMC7966164.

35. Gliebus GP. Memory Dysfunction. Continuum (Minneap Minn). 2018;24(3, BEHAVIORAL NEUROLOGY AND PSYCHIATRY):727–744. https://doi.org/10.1212/CON.0000000000000619. PMID: 29851875.

36. Berron D, van Westen D, Ossenkoppele R, Strandberg O, Hansson O. Medial temporal lobe connectivity and its associations with cognition in early Alzheimer's disease. Brain. 2020;143(4):1233–1248. https://doi.org/10.1093/brain/awaa068. Erratum in: Brain. 2021;144(9):e84. PMID: 32252068; PMCID: PMC7174043.

37. Wu YJ, Wu N, Huang X, Rao J, Yan L, Shi L, Huang H, Li SY, Zhou FQ, Wu XR. Evidence of cortical thickness reduction and disconnection in high myopia. Sci Rep. 2020;10(1):16239. https://doi.org/10.1038/s41598-020-73415-3. PMID: 33004887; PMCID: PMC7530748.

38. Huang X, Hu Y, Zhou F, Xu X, Wu Y, Jay R, Cheng Y, Wang J, Wu X. Altered whole-brain gray matter volume in high myopia patients: a voxel-based morphometry study. NeuroReport. 2018;29(9):760–7. PMID: 29634585; PMCID: PMC5965935.

39. Wang H, Wen H, Li J, Chen Q, Li S, Wang Y, Wang Z. Characterization of Brain Microstructural abnormalities in High Myopia patients: a preliminary Diffusion Kurtosis Imaging Study. Korean J Radiol. 2021;22(7):1142–51. https://doi.org/10.3348/kjr.2020.0178. Epub 2021 May 4. PMID: 33987989; PMCID: PMC8236370.

40. YIN Y. Diffusion Tensor imaging study of white matter structure in preschool children with autism[D]. Guangzhou: Southern Medical University; 2021. https://doi.org/10.27003/d.cnki.gojyu.2021.000018.

41. Lanciego JL, Luquin N, Obeso JA. Functional neuroanatomy of the basal ganglia. Cold Spring Harb Perspect Med. 2012;2(12):a009621. https://doi.org/10.1101/cshperspect.a009621. PMID: 23071379; PMCID: PMC3543080.

42. Vatansever D, Manktelow AE, Sahakian BJ, Menon DK, Stamatakis EA. Cognitive flexibility: a default network and basal ganglia connectivity perspective. Brain Connect. 2016;6(3):201–7. https://doi.org/10.1089/brain.2015.0388. Epub 2016 Feb 16. PMID: 26652748; PMCID: PMC5118962.

43. Yeo BT, Krienen FM, Sepulcre J, Sabuncu MR, Lashkari D, Hollinshead M, Roffman JL, Smoller JW, Zöllei L, Polimeni JR, Fischl B, Liu H, Buckner RL. The organization of the human cerebral cortex estimated by intrinsic functional connectivity. J Neurophysiol. 2011;106(3):1125–65. https://doi.org/10.1152/jn.00338.2011. Epub 2011 Jun 8. PMID: 21653723; PMCID: PMC3174820.

44. Androulakis XM, Krebs KA, Jenkins C, Maleki N, Finkel AG, Rorden C, Newman R. Central Executive and Default Mode Network Intranet work functional connectivity patterns in chronic migraine. J Neurol Disord. 2018;6(5):393. https://doi.org/10.4172/2329-6895.1000393. Epub 2018 Oct 17. PMID: 30574520; PMCID: PMC6298435.

45. Wang X, Zhang W, Sun Y, Hu M, Chen A. Aberrant intra-salience network dynamic functional connectivity impairs large-scale network interactions in schizophrenia. Neuropsychologia. 2016;93(Pt A):262–70. Epub 2016 Nov 5. PMID: 27825906.

46. Gong G, He Y, Chen ZJ, Evans AC. Convergence and divergence of thickness correlations with diffusion connections across the human cerebral cortex. NeuroImage. 2012;59(2):1239–48. https://doi.org/10.1016/j.neuroimage.2011.08.017. Epub 2011 Aug 22. PMID: 21884805.

Publisher's Note